A Thermal Hydraulic Model of Melt Lubrication in Railgun Armatures

R. E. Kothmann and F. Stefani

Institute for Advanced Technology
The University of Texas at Austin

March 2003

IAT.R 0214

IAT Institute for Advanced Technology
The University of Texas at Austin

The views, opinions, and/or findings contained in this report are those of the author(s) and should not be construed as an official Department of the Army position, policy, or decision, unless so designated by other documentation.

REPORT DOCUMENTATION PAGE

Form Approved
OMB NO. 0704-0188

1. AGENCY USE ONLY (Leave blank)	2. REPORT DATE	3. REPORT TYPE AND DATES COVERED
	March 2003	Technical Report

4. TITLE AND SUBTITLE
A Thermal Hydraulic Model of Melt Lubrication in Railgun Armatures

5. FUNDING NUMBERS
Contract # DAAD17-01-D-0001

6. AUTHOR(S)
R. E. Kothmann and F. Stefani

7. PERFORMING ORGANIZATION NAME(S) AND ADDRESS(ES)
Institute for Advanced Technology
The University of Texas at Austin
3925 W. Braker Lane, Suite 400
Austin, TX 78759-5316

8. PERFORMING ORGANIZATION REPORT NUMBER
IAT.R 0214

9. SPONSORING / MONITORING AGENCY NAME(S) AND ADDRESS(ES)
U.S. Army Research Laboratory
ATTN: AMSRL-WM-B
Aberdeen Proving Ground, MD 21005-5066

10. SPONSORING / MONITORING AGENCY REPORT NUMBER

11. SUPPLEMENTARY NOTES
The views, opinions, and/or findings contained in this report are those of the author(s) and should not be considered as an official Department of the Army position, policy, or decision, unless so designated by other documentation.

12a. DISTRIBUTION / AVAILABILITY STATEMENT
Approved for public release; distribution unlimited.

12b. DISTRIBUTION CODE
A

13. ABSTRACT *(Maximum 200 words)*
This paper describes the first step toward a model of the liquid film at the rail/armature interface in solid armature railguns. It considers high-speed Couette flow with purely viscous heating and does not include MHD body forces or Joule heating. The focus is on coupled fluid dynamics and multi-phase heat transfer. The formulation is similar to the analysis of melt lubrication in rotating projectile bands, but our first principles model allows the possibility of solidification while the armature is passing, a feature that has been missing from previous analyses. The model is moderately successful at reproducing results of experiments which measured high-speed mechanical wear of 7075 aluminum sliding against ETP copper for face pressures ranging from 6 to 22 ksi. Discrepancies between calculated and experimental results are attributed to uncertainties in modeling the complex phase change behavior of aluminum alloy 7075 and uncertain conditions at the rail interface.

14. SUBJECT TERMS
melt lubrication, railgun armatures

15. NUMBER OF PAGES
25

16. PRICE CODE

17. SECURITY CLASSIFICATION OF REPORT	18. SECURITY CLASSIFICATION OF THIS PAGE	19. SECURITY CLASSIFICATION OF ABSTRACT	20. LIMITATION OF ABSTRACT
Unclassified	Unclassified	Unclassified	UL

TABLE OF CONTENTS

LIST OF FIGURES

LIST OF TABLES

A THERMAL HYDRAULIC MODEL OF MELT-LUBRICATION IN RAILGUN ARMATURES

R. E. Kothmann
Kothmann Consulting, Pittsburgh, Pennsylvania

F. Stefani
Institute for Advanced Technology, Austin, Texas

Abstract—This paper describes the first step towards a model of the liquid film at the rail/armature interface in solid armature railguns. The model considers high-speed Couette flow with purely viscous heating and does not include MHD body forces or Joule heating. The focus of the model is on coupled fluid dynamics and multi-phase heat transfer. The formulation is similar to the analysis of melt lubrication in rotating projectile bands. However, our first principles model allows the possibility of solidification while the armature is passing, a feature that has been missing from previous analyses. The model is moderately successful at reproducing results of experiments which measured high-speed mechanical wear of 7075 aluminum sliding against ETP copper for face pressures ranging from 6 to 22 ksi. Discrepancies between calculated and experimental results are attributed to uncertainties in modeling the complex phase change behavior of aluminum alloy 7075 and uncertain conditions at the rail interface.

INTRODUCTION

The normal operation of a solid armature railgun necessarily involves melting and loss of aluminum from the armature. This is evident from the coating of solidified aluminum that is left on rails practically from the starting position of the armature. Excessive or uneven loss of aluminum from the armature is not desirable because it can lead to arcing contact. However, there is reason to believe that some loss of aluminum, sufficient to maintain a stable, liquid film interface, has several benefits: it provides an uniform, low-voltage electrical contact between rail and armature, it reduces the frictional drag force between armature and rail, and there is evidence to suggest that it suppresses the onset of gouging by several hundred meters per second [1].

There are several processes by which aluminum is removed from the armature. Most armature wear models to date have focused on "current melt wave" behavior, whereby intense skin-effect heating leads to localized melting and loss of aluminum at the perimeter of the rail/armature interface [2-7]. When the armature is moving faster than 700 to 1000 m/s, however, the root cause of wear is not obvious, since at this point mechanical (viscous heat generation) and electrical heating are both potentially significant.

The importance of mechanical heating or "melt lubrication" as a wear mechanism in railguns was demonstrated in a series of tests conducted at the Institute for Advanced Technology in 1997 [8]. The tests measured the wear rate of 7075 aluminum alloy in high-speed sliding contact with ETP copper. In these tests, small sliders were accelerated from rest to 2200 m/s while maintaining a steady contact pressure throughout most of the launch. Pressures ranged from 6.5

ksi to 21.8 ksi. Even though the tests were conducted using a railgun, they measured purely mechanical (frictional and viscous) components of wear by electrically isolating the sliders from the current path. The tests found that, at pressures typical of armature/rail contact, wear due to mechanical heating was comparable to the wear rate measured in armatures.

The results were originally presented as a set of five curves showing measured depth of wear vs. distance traveled. The same data are shown in Figure 1, plotted in a form that is more easily compared to the output of the model we propose. The figure plots the velocity at which the slider is wearing (Melt Front Velocity) against the speed of the slider in the experiments. The data do not extend below 800 m/s because, until the sliders enter into a state of melt lubrication, there is no measurable wear.

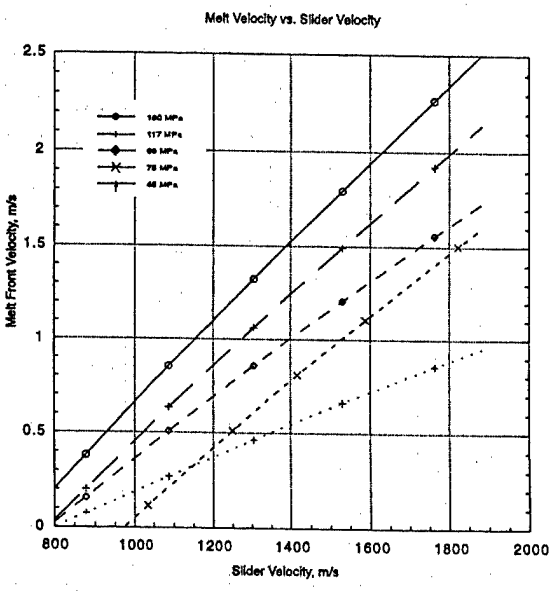

Fig. 1. Curves obtained from wear tests of 7075 aluminum in sliding contact with ETP copper [8].

DERIVATION OF MODEL

Derivation of Equations

Nomenclature Table.

C_u	constant in solution for U(Y)	u, v, w	velocity in x, y, z directions
c, c_r, c_s	specific heat of melt, rail, slider	u_1, u_2	components of u
Ec	Eckert number	v_o	melt film velocity at slider interface
F_y	normal force on the slider	v_{ms}	melting rate into the slider
H_m	latent heat of melting	X	position of re-solidification/melt interface
h	film thickness	x	direction of slider motion
k, k_r, k_s	thermal conductivity of melt, rail, slider	Y	dimensionless coordinate
L_s	smaller side of the slider	y	direction ⊥ to melt plane
L_x,L_z	slider dimensions in x and z directions	z	direction in melt plane ⊥ to x
m_o	mass melt rate per unit area	Z	dimensionless coordinate
n	index	β	ratio of longer to shorter side of slider
Pr	Prandtl number	δ	average pressure factor
p	pressure	ζ	fraction of melt solidified under the slider
t, t_r, t_s	temperature of melt, rail, slider	θ	dimensionless temperature in melt film
t_{im}	incipient melting temperature of slider	κ, κ_r, κ_s	thermal diffusivity in melt, rail, slider
t_L	liquidus temperature of slider	λ	solidification rate parameter
t_m	melting temperature	μ	absolute viscosity of melt film
t_m'	pseudo melt temperature	ρ, ρ_r, ρ_s	density of melt, rail, slider
t_{r_o}	initial temperature of rail	σ	load per unit area
U, V, W	dimensionless velocity in x, y, z directions	τ	time

Our model is based on a model of melt lubrication by Stiffler [9], as shown in Figure 2a. The model assumes a block of length L_x and width L_z moving at a constant x-directed velocity u_0. A steady force normal to the rail $F_y = A\sigma = \sigma L_x L_z$ is applied to the block. Viscous heating causes the slider to melt at a constant melt velocity v_{ms}. The film has a constant and uniform thickness h.

Figure 2b illustrates the model proposed for the railgun armature. It is based on the same assumption made by Stiffler with the exception that the film material is allowed to solidify. This is reflected in the italicized text in assumption (4) below.

1. The fluid is laminar and incompressible.
2. As per standard lubrication theory, the pressure is constant through the thickness of the film and average values of density and viscosity are employed.
3. Film thickness and melt penetration into the solid are small compared to the length and width of the slider.
4. Only one surface is melting. *Solidification can occur on the stationary surface during transit of the slider.*
5. Quasi steady-state conditions are reached in the film. That is, we are solving for a set of average conditions over the length and width of the contact face.

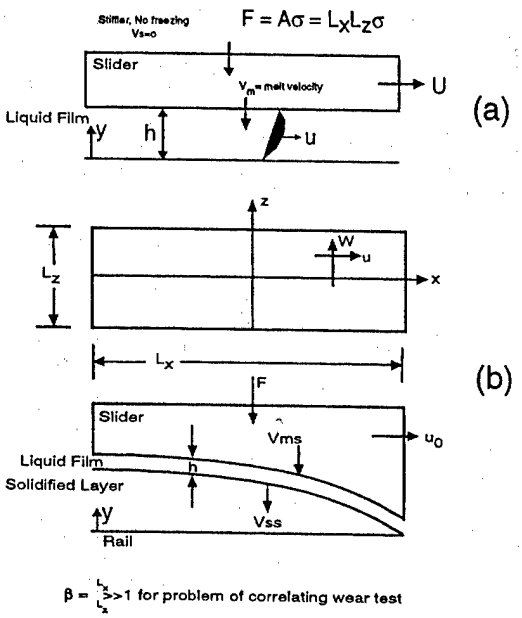

Fig. 2. (a) Schematic of melt lubrication model by Stiffler; (b) our model is based on Stiffler's but allows solidification under the slider.

Assumption (3) is justified by the experimental finding that the thickness of the film is on the order of 20 microns or less [8]. The film thickness of 20 microns or less is appreciably smaller than the smallest dimension of the slider (1.4 mm) and the thermal diffusion depth into the slider, which is on the order of 50 microns. Viscosity is approximately constant because there is very little variation in temperature across the film, and furthermore, the change in viscosity of liquid aluminum with temperature is small.

The assumption that only one surface is melting is consistent with evidence that rails are not melting. On the other hand, the assumption that the film can solidify marks the principal difference in our approach and is a key feature of our model. Additionally, Stiffler neglects the effect of mass injection on anything but the squeeze film velocity; we include the effect of injection on the velocity profile in a way that affects dissipation in the film and heat transfer to the boundaries. A thermal model of the melt/rail interface is used to determine whether solidification occurs and at what rate.

An additional assumption we make is that acceleration is insignificant. In the experiments, the sliders were accelerated at 10^6 m/s^2 [8]. The principal effect of acceleration is to produce a "lag" in the Couette profile, that is, there is a time required for the velocity distribution to adjust to the changing speed. The lag is on the order of a few microseconds, during which the velocity changes by a fraction of a percent. Acceleration can thus be neglected because the velocity profile is lagging by only a small fraction of the velocity.

Our derivation follows closely that of Stiffler and the basic equations for thin films. Following Stiffler, variables and parameters pertaining to the liquid film are not subscripted whereas those pertaining to the slider and rail are.

MOMENTUM AND CONTINUITY EQUATIONS

The momentum equations for the x and z directions are (steady state, with $\frac{dp}{dy} = 0$)

$$\rho u\frac{\partial u}{\partial x} + \rho v\frac{\partial u}{\partial y} + \rho w\frac{\partial u}{\partial z} + \frac{\partial p}{\partial x} = \frac{\partial}{\partial y}(\mu\frac{\partial u}{\partial y}) \tag{1}$$

$$\rho u\frac{\partial w}{\partial x} + \rho v\frac{\partial w}{\partial y} + \rho w\frac{\partial w}{\partial z} + \frac{\partial p}{\partial z} = \frac{\partial}{\partial y}(\mu\frac{\partial w}{\partial y}) \tag{2}$$

Assume $u = u_1(y) + u_2(x,y,z)$, with $|u_1| \rangle\rangle |u_2|$, where u_1 is the Couette flow velocity with injection and u_2 is the "squeeze film" component of velocity. Then, applying equation (1) to u_1 and u_2

$$\rho u\frac{\partial u_1}{\partial x} + \rho v\frac{\partial u_1}{\partial y} + \rho w\frac{\partial u_1}{\partial z} = \frac{\partial}{\partial y}(\mu\frac{\partial u_1}{\partial y}) \tag{3}$$

and

$$\rho u\frac{\partial u_2}{\partial x} + \rho v\frac{\partial u_2}{\partial y} + \rho w\frac{\partial u_2}{\partial z} + \frac{\partial p}{\partial x} = \frac{\partial}{\partial y}(\mu\frac{\partial u_2}{\partial y}). \tag{4}$$

Note that equation (3) describes conditions for Couette flow with $\frac{dp}{dx} = 0$. Thus

$$u_1 = u_0 @ y = h$$

$$U_1 = 0 @ y = 0$$

Also, since u_1 is independent of x and z, and μ is assumed constant, equation (3) simplifies to

$$\rho v\frac{du_1}{dy} = \mu\frac{d^2u_1}{dy^2} \tag{5}$$

For thin films, equations (2) and (4) can be simplified by neglecting all terms on the left hand side except $\frac{dp}{dx}$ and $\frac{dp}{dy}$. Both w and u_2 are assumed to be independent of x and the pressure gradients due to momentum convection are small compared to the viscous forces. Then (2) and (4) become, respectively

$$\frac{dp}{dz} = \mu\frac{d^2w}{dy^2} \tag{6}$$

$$\frac{dp}{dx} = \mu\frac{d^2u_2}{dy^2} \tag{7}$$

which can be integrated to obtain

$$u_2 = \frac{1}{2\mu}(y^2 - yh)\frac{\partial p}{\partial x} \tag{8}$$

$$w = \frac{1}{2\mu}(y^2 - yh)\frac{\partial p}{\partial z} \tag{9}$$

At this point, it is convenient to introduce a new variable ζ, the fraction of the melted material that solidifies. (1- ζ) is the fraction that leaves at the sides of the slider. Equations 8 and 9 show that the squeeze film flow has a parabolic profile in both lateral directions. Applying the continuity equation to the melt film at distance y from the rail (or solidified interface) with the overall fraction $1-\zeta$ leaving all four sides with the parabolic profiles for u_2 and w gives

$$v = v_0(\zeta + (1-\zeta)(3-2\frac{y}{h})(\frac{y}{h})^2) \tag{10}$$

where $v_0 = \frac{m_0}{\rho}$. The fraction ζ is determined from the heat transfer analysis. Then

$$u = u_1(y) + u_2(x, y, z) = u_1(y) + \frac{1}{2\mu}(y^2 - yh)\frac{\partial p}{\partial x} \tag{11}$$

where u_1 is obtained from numerical integration of equation (5). The solution of equation (5) is obtained based on h=constant, and it is assumed that v is a function of y only.

THE FILM REYNOLDS EQUATION

The continuity equation for the film is

$$\frac{\partial}{\partial x}(\rho u) + \frac{\partial}{\partial y}(\rho v) + \frac{\partial}{\partial z}(\rho w) = 0 \tag{12}$$

Substituting $u, v,$ and w from above and integrating over the height of the film gives

$$\frac{\partial}{\partial x}(\frac{-\rho h^3}{12\mu}\frac{\partial p}{\partial x}) + \frac{\partial}{\partial z}(\frac{-\rho h^3}{12\mu}\frac{\partial p}{\partial z}) = \frac{-\partial}{\partial x}[\int_0^h \rho u_1(y)dy] + \rho v_0(1-\zeta) \tag{13}$$

For a uniform thickness film,

$$\nabla^2 p = \frac{-12 m_0(1-\zeta)\mu}{\rho h^3} \tag{14}$$

This is the same relation as found by Stiffler, [9] except for the 1-ζ factor which accounts for solidification. The film thickness is given by

$$h^3 = \frac{\mu m_0 (1-\zeta) L_s^2 \delta}{\rho \sigma} \tag{15}$$

where the average pressure parameter, δ, is [10]

σ=mean normal pressure on film = F_z/A
L_s=smaller of L_x and L_z

$$\delta = 1 - \frac{192}{\pi^5 \beta} \sum_{n=1,3,5}^{\infty} n^{-5} \tanh(n\pi\beta/2) \tag{16}$$

β=Ratio of the longer side of the slider to the shorter side of the slider.

DIMENSIONLESS VARIABLES

The equations are rewritten in nondimensional form to reduce the number of parameters and obtain solutions in terms of classical nondimensional quantities. The x momentum equation, equation (5), is made dimensionless by

$$V = \frac{v}{v_0}, \quad U_1 = \frac{u_1}{u_0}, \quad Y = y/h. \tag{17}$$

Because U_1 is only a function of Y, the result is written as an ordinary differential equation,

$$\frac{d^2 U_1}{dY^2} - \mathrm{Re}_w V \frac{dU_1}{dY} = 0 \tag{18}$$

$$\text{where } \mathrm{Re}_w = \rho \frac{v_0 h}{\mu}. \tag{19}$$

The Y velocity can be rewritten as

$$V = -(\zeta + (1-\zeta)(3Y^2 - 2Y^3)) \tag{20}$$

The first integration is performed using an integration factor to give

$$\frac{dU_1}{dY} = C_u \, e^{+\int_0^Y \mathrm{Re}_w V dY} \tag{21}$$

where C_u is a constant to be determined by the boundary conditions, namely,

$$U_1 = 0 \,@\, Y = 0 \tag{22}$$

$$U_1 = 1 @ Y = 1 \tag{23}$$

Equation (21) was integrated numerically using a fourth order Runge-Kutta method. The resulting values of $U_1(Y)$ and $\frac{dU_1}{dY}$ are used in the energy equation.

ENERGY EQUATION

The boundary layer formulation of the steady state energy equation for the liquid film with constant specific heat and thermal conductivity is [11].

$$\rho c u \frac{\partial t}{\partial x} + \rho c v \frac{\partial t}{\partial y} + \rho c w \frac{\partial t}{\partial z} = k \nabla^2 t + u \frac{dp}{dx} + \mu \phi \tag{24}$$

where the dissipation function ϕ is

$$\phi = (\frac{\partial u}{\partial y})^2 + (\frac{\partial w}{\partial y})^2 \tag{25}$$

Because the temperature is assumed to be a function of y only and both $u\frac{dp}{dx}$ and $(\frac{\partial w}{\partial y})^2$ can be neglected, the energy equation simplifies to

$$\rho c v \frac{dt}{dy} = k \frac{\partial^2 t}{\partial y^2} + \mu (\frac{du}{dy})^2 \tag{26}$$

We make the energy equation dimensionless using equation (17) and

$$\theta = \frac{t}{t_m} - 1 \tag{27}$$

where t_m is the melting temperature. The result is

$$\frac{d^2\theta}{dY^2} = V \mathrm{Re}_w \Pr \frac{d\theta}{dY} - \Pr Ec (\frac{dU_1}{dY})^2 \tag{28}$$

where u_2 has been neglected as compared to u_1 and where

$$Ec = \frac{u_0^2}{ct_m} \tag{29}$$

$$\Pr = \frac{\mu c}{k} \tag{30}$$

BOUNDARY CONDITIONS FOR THE ENERGY EQUATION

A total of four boundary conditions must be matched when solving the liquid film energy equation. These are:

1. $\theta(1) = 0$. The liquid/ slider interface must be at the melting point.
2. The heat flux from the liquid must supply the melt rate energy and heat conduction to the slider.
3. With solidification the liquid interface must be at the melting temperature, $\theta(0)=0$. Without solidification, the film temperature must equal that of the rail and $\theta(0)$ must be greater than zero.
4. With solidification, the heat flux from the liquid plus the solidification energy flux must match heat conduction to the resolidified layer. Without solidification, the heat flux from the film must match the flux to the rail.

Boundary Condition 2

Following Stiffler [9], it is assumed that the melting rate at the slider has reached its steady state rate where the flux is given by [12]

$$q_m = \rho v_0 [H_m + c_s(t_m - t_0)] \tag{31}$$

where H_m is the heat of fusion. Thus, the dimensionless heat flux boundary condition at Y=1 becomes

$$[\frac{d\theta}{dY}]_{Y=1} = -\mathrm{Re}_w \,\mathrm{Pr}[\frac{H_m}{ct_m} + (1 - \frac{t_0}{t_m})\frac{c_s}{c}] \tag{32}$$

The boundary condition at the rail side of the liquid film is more complex. The two cases, solidification and no solidification, are considered separately.

No Solidification on Rail under Slider

The temperature and heat fluxes at the rail/liquid interface must match and the interface temperature must be above the melting point. The heat flux to the rail is taken to be the average over the contact time. The heat flux is obtained for the case when the rail surface undergoes a step change to the temperature of the film interface. From Carslaw and Jaeger [13], the average heat flux into a semi-infinite solid from $\tau = 0$ to $\tau = L_x / u_0$ for step change from t_{r_o} to $t_r(0)$ is

$$q_r = \frac{2k_r(t_r(0) - t_{r_o})}{\sqrt{\pi \kappa_r (\frac{L_x}{u_0})}} \tag{33}$$

The heat flux boundary condition at the rail/liquid interface is then

$$[\frac{d\theta}{dY}]_{Y=0} = \frac{2k_r}{k}(\frac{t_m(1+\theta(0)) - t_{r_0})}{t_m\sqrt{\frac{\pi\kappa_r L_x}{u_0}}}) \qquad (34)$$

where $t_r(0) = [1+\theta(0)]t_m$.

SOLIDIFICATION ON RAIL UNDER THE SLIDER

An additional interface is formed when solidification occurs, but its boundary conditions are included in the solidification solution. The approach is similar to the case for no solidification but uses the solution for a liquid which is above the melting temperature that comes into contact with a cold solid (see Appendix A).

METHOD OF SOLUTION

Once one has assumed a value for v_{ms} and ζ, one can calculate the film thickness for the given slider dimensions, pressure, and velocity. One can also integrate the x momentum equation to obtain values of U_1 and $\frac{dU_1}{dY}$. Because the two interface conditions at the slider, conditions (1) and (2), are also known, one can integrate the second order energy equation starting at Y=1 and proceeding to Y=0. Note that both initial value and slope are available at Y=1. The result of the integration will be for $\theta(0)$ and $\frac{d\theta(0)}{dY}$. The iteration is completed first for no solidification. For no solidification, one keeps $\zeta = 0$ and changes v_{ms} until the heat flux from the film matches the heat flux to the rail for the value of $\theta(0)$. If the value of $\theta(0)$ is greater than 0 when the fluxes match, there is no solidification and the solution is finished. Otherwise, one begins the iteration for solidification.

For solidification on the rail, one must first find a non-zero value of ζ needed to satisfy the boundary condition (3), $\theta(0) = 0$. If $\theta(0)$ is not zero, then the assumed value of ζ is adjusted until it is zero. When this has been accomplished, only boundary condition (4) remains to be satisfied. A value of t_v is assumed and λ is obtained from the solidification solution along with the values of X and of the heat flux at the interface. The value of t_v is adjusted until the flux at the solidified surface/film interface matches the flux from the film solution. When the heat fluxes at the solidified boundary match, it is then determined if the value of X is too high or too low to match the assumed solidification fraction, ζ. If not, v_m is adjusted accordingly, and the procedure is repeated until the solidification rates also match.

RESULTS

The model is run with the objective of reproducing the experimental results described in the introduction of this paper. Three slider pressures are considered 10.9, 17.0, and 21.8 ksi, which

effectively bracket the data at pressures characteristic of railgun armatures. For each value of pressure, solutions are found for slider speeds ranging from 800 m/s to 1800 m/s using the parameters and properties shown in Table 1. We used the incipient melting temperature, 805 K, as the melting temperature.

Table 1.

Symbol	Variable Name	Physical Quantity	Value	Units
ρ	RHOL	Density of liquid	2485	kg/m^3
κ	CONDKL	Thermal conductivity of liquid	83.7	W/m/K
μ	MU	Absolute viscosity of liquid	0.00450	Ns/m^2
ρ_r	RHOR	Density of rail	8950	kg/m^3
κ_r	CONDKR	Thermal conductivity of rail	374	W/m/K
ρ_s	RHOS	Density of slider	2800	kg/m^3
κ_s	CONDKS	Thermal conductivity of slider	170	W/m/K
c	CPL	Specific heat of liquid	1084	J/kg/K
c_r	CPR	Specific heat of rail	400	J/kg/K
c_s	CPS	Specific heat of slider	1200	J/kg/K
H_m	HM	Latent heat of melting of slider	3.78×10^5	J/kg
L_x	LZ	Length of slider	0.0155	m
L_z	LX	Width of slider	0.0014	m
t_{im}	TINSM	Incipient melting temperature of slider	805	K
t_L	TLIQ	Liquidus temperature of slider	908	K
t_m	TM	Melting temperature of slider	805	K

MELT VELOCITY, ORIGINAL MODEL

A direct comparison between model and experiment is obtained by comparing Figure 3, which plots calculated melt velocity v_{ms} vs. slider speed, with experimental curves in Figure 1. Although the model predicts melt velocities that are centered within the range of experimental values (v_{ms}=1.1 m/s), the model fails to reproduce the strong dependence on velocity and pressure observed in the experiments.

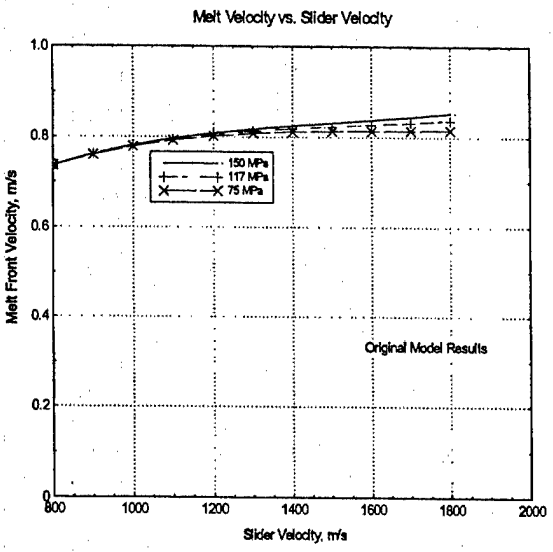

Fig. 3. Initial results for three values of pressure. The relative insensitivity of the model to velocity and pressure shows poor agreement with experiment.

The relative insensitivity of the model to velocity and pressure can be attributed to the solidification boundary condition (4) coupled with the fact that residence time is inversely proportional to the speed of the slider. Although there is an increased average heat transfer rate (transient conduction into the rail), there is less solidification under the slider as speed increases. Reduced solidification at high speeds means that the film has to get thicker, which prevents viscous dissipation from increasing appreciably. This strong self-limiting effect is a feature of the laminar model with high solidification rates. The fraction of melt solidified under the slider ranged from 81.5 to 99.7 percent over the range of conditions in Figure 3.

The small temperature rise in the film also indicated a problem with the model when we reconsidered the large range between the incipient melting temperature and the liquidus temperature. The peak temperature in the film of 817 K, which is 12 K above the incipient melting temperature and 92 K below the liquidus temperature, is inconsistent with the assumption that the full latent energy has been absorbed by the molten aluminum.

REVISED MODEL

This realization motivated us to include a more realistic approximation to the complex phase change behavior of 7075 aluminum alloy. We also reasoned that lowering the energy needed to release aluminum into the film ought to increase the melt speed v_{ms}. Additionally, we reasoned that the viscosity near the incipient melting temperature should be much higher than that of liquid aluminum. Appendix B describes our effort to incorporate a description of distributed latent heat into our model. As a brief summary of the revised model, we kept approximately 10 percent of the latent heat at a temperature of 815 K, 10 K above the incipient melting point. The remainder of the latent heat was assumed uniformly distributed over the range from 815 to 908 K, the liquidus temperature.

We also attempted to develop an appropriate model of the viscosity of the partially liquid state of 7075 aluminum between 805 and 908 K. The variable viscosity model is also described in Appendix B. The model was ultimately discarded because the effect of decreasing viscosity with increasing temperature predicted a smaller increase in melt velocity with slider speed than resulted from a constant viscosity.

The melt velocity results for the revised model are shown in Figure 4. As expected, the rate of melting was increased, but the rates were still not very sensitive to pressure or slider velocity.

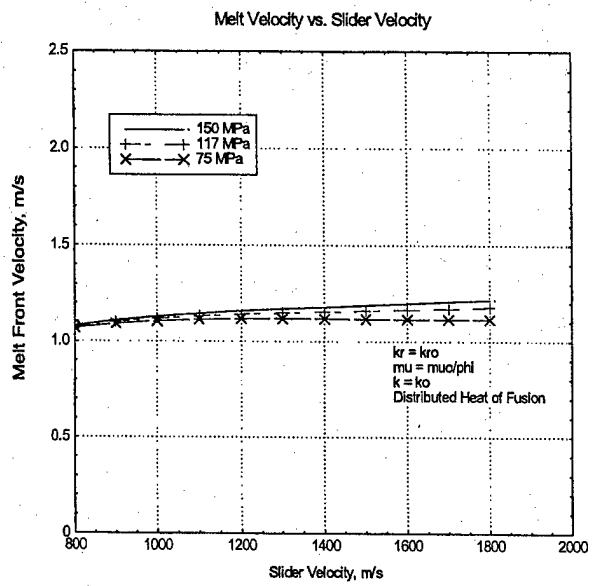

Fig. 4. Results of model revised to include a more realistic approximation to the phase change behavior of 7075 aluminum alloy and a model of temperature-dependent model of viscosity. As expected, the rate of melting increased but the rates are not very sensitive to pressure or slider velocity.

MODEL INADEQUACIES

The poor agreement indicates that one or more of the assumptions made in the model is incorrect. We examined several of the assumptions that appeared to be most questionable. These include: (1) perfect thermal contact between film and rail, (2) laminar flow of the film, and (3) simple melting of the aluminum alloy.

We first explored the effect of a thermal interface resistance between the film and the rail. Early experimental work on liquid metal heat transfer was unable to confirm the high heat transfer rates predicted at low Prandtl numbers. It turned out that interface resistance due to very thin oxide layers and non-wetting greatly reduced the heat transfer from the theoretical rates. The same effect might be present in the railgun environment. It could be caused by similar phenomena or by gases entrained as the slider advances.

Because our formulation could not readily be modified to include this in the boundary condition, we approximated the effect by reducing the thermal conductivity of the rail. A reduction of thermal conductivity of the rail by a factor of ten results in a reduction of heat transfer to the rail

by about a factor of three. Results still exhibited the same trends as before for the nominal liquid viscosity.

Another issue that arose was the validity of the laminar flow assumption. Early calculations using Stiffler's model without solidification indicated that the film could be expected to be in a turbulent flow regime. In most of our program data runs, the Reynolds number for the film reached the turbulent transition at the higher slider velocities. We decided to approximate the effects of turbulence by increasing the eddy diffusivity of heat and momentum. We applied a factor to increase both the viscosity and thermal conductivity by a uniform amount across the width of the channel. When we combined this with the reduced heat transfer to the rail, we obtained results that closely followed the major trends of the test data.

Examples of the results are shown in Figures 5 and 6. In Figure 5, the rail thermal conductivity is reduced by a factor of ten and the viscosity and thermal conductivity of the melt film are each increased by a factor of three. The curve for σ = 10.9 ksi agrees very well with the test data in Figure 1 between 1300 and 1800 m/s. Figure 6 is for the conditions with rail thermal conductivity reduced by a factor of 15, and both viscosity and thermal conductivity of the melt increased by a factor of four. The curve in Figure 6 for σ = 21.8 ksi is in very good agreement with the test data from 1000 to 1800 m/s.

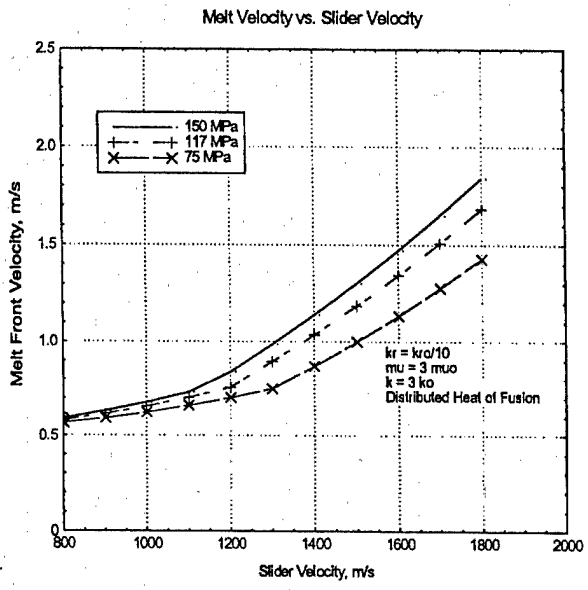

Fig. 5. Results of model revised to (1) suppress heat transfer to the rails by reducing the thermal conductivity of the rails by a factor of 10 and, (2) approximate turbulence by increasing viscosity and conductivity by a factor of three. The change in slope between 1100 and 1300 m/s corresponds to the end of melt solidification under the slider. Above 1300 m/s, the trends agree well with the data.

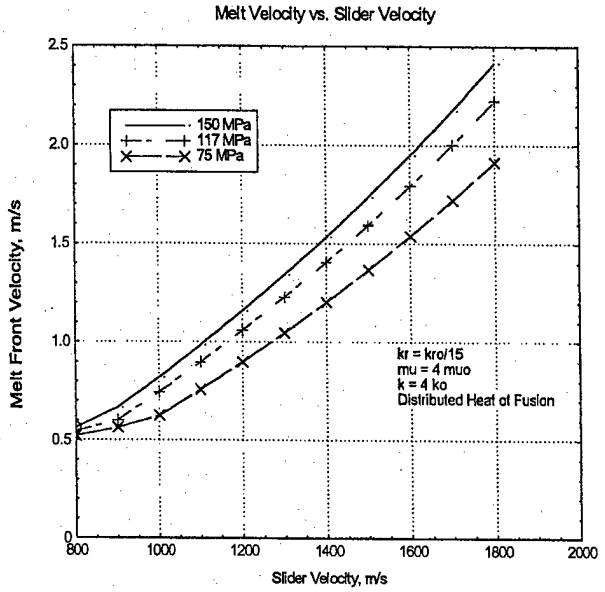

Fig. 6. Results of the model revised to (1) suppress heat transfer to the rails by reducing the thermal conductivity of the rails by a factor of 15 and, (2) approximate turbulence by increasing viscosity and conductivity by a factor of four. The changes in slope at 900 to 1000 m/s correspond to the end of melt solidification under slider. Good agreement with experiments above the changes in slope suggests that the film does not solidify under the armature.

A change in slope is seen in Figure 5 at slider velocities between 1100 and 1300 m/s. Above this change in slope, the trend agrees well with the test data. In Figure 6, the slope changes occur between 900 and 1000 m/s. Again the trends agree well above the change. The change in slope corresponds to the end of melt solidification under the slider, suggesting that the film does not solidify under the armature at all.

DISCUSSION

There are several observations that can be made.

1. The model results do not apply for slider velocities below approximately 1000 m/s. This is believed to be due to the transient nature of the railgun-driven wear experiments. In a separate analysis of solid-solid sliding, we found that the melting temperature is reached at about the time the velocity reaches 700 m/s for an acceleration of 10^6 m/s^2. Thus, we do not expect the assumption of quasi-steady-state melt to be satisfied until a velocity of 1000 m/s is reached.

2. Reduced heat transfer to the rail combined with higher viscosity and thermal conductivity of the melt film provides a better fit to the data. A reduction in rail heat transfer due to interface thermal resistance of a factor of three to four appears to be needed. Effective viscosity and thermal conductivity higher than their nominal liquid values by a factor of three to four also appear to be needed. Viscosity could be explained either by turbulence or by incomplete melting because the maximum liquid film temperature was below the liquidus temperature for all conditions in Figures 5 and 6.

3. The results are not highly sensitive to the location of the pseudo melting point, so long as it is within 20 percent of the incipient melting temperature.

The results give encouragement that a valid model can be developed. The model clearly indicates that film solidification under the armature is not an important process. Future work should focus on modifying the analysis to include:

- turbulent correlations of eddy viscosity and eddy diffusivity,
- additional information on viscosity and the distribution of heat of transformation in the range between the incipient melting and liquidus temperatures,
- the effect of thermal interface resistance between the film and the rail.

The complexities of resolidification can be avoided in future work.

ACKNOWLEDGMENT

The authors thank Dr. Jerry Parker for many useful discussions.

The research reported in this document was performed in connection with Contract number DAAD17-01-D-0001 with the U.S. Army Research Laboratory. The views and conclusions contained in this document are those of the authors and should not be interpreted as presenting the official policies or position, either expressed or implied, of the U.S. Army Research Laboratory or the U.S. Government unless so designated by other authorized documents. Citation of manufacturer's or trade names does not constitute an official endorsement or approval of the use thereof. The U.S. Government is authorized to reproduce and distribute reprints for Government purposes notwithstanding any copyright notation hereon.

REFERENCES

[1] F. Stefani and J.V. Parker, "Experiments to Measure Gouging Threshold Velocity for Various Metals Against Copper," *IEEE Trans. Magnetics*, vol. 35, no. 1, pp. 312-316, January 1999.

[2] J.P. Barber, A. Challita, B. Maas, and L. Thurmond, "Contact Transition in Metal Armatures," *IEEE Trans. on Magnetics*, vol. 27, no. 1, pp. 228-232, January 1991.

[3] J. P. Barber and A. Challita, "Velocity Effects on Metal Armature Contact Transition," *IEEE Trans. on Magnetics*, vol. 29, no. 1, pp. 733-37, January 1993.

[4] P.B. Parks, "Current Melt-Wave Model for Transitioning Solid Armature," *J. Appl. Phys.*, vol. 67, no. 1, pp. 3511-16, April 1990.

[5] T.E. James, "Current Wave and Magnetic Saw-Effect Phenomena in Solid Armature," *IEEE Trans. on Magnetics*, vol. 31, no. 1, pp. 622-627, January 1995.

[6] J.P. Barber and Y.A. Dreizin, "Model of Contact Transitioning with 'Realistic' Armature Rail Interface," *IEEE Trans. on Magnetics*, vol. 31, no. 1, pp. 96-100, January 1995.

[7] L.C. Woods, "The Current Melt Wave Model," *IEEE Trans. on Magnetics*, vol. 32, no. 1, January 1997.

[8] F. Stefani and J.V. Parker, "Experiments to Measure Wear in Aluminum Armatures," *IEEE Trans. Magnetics*, vol. 35, no. 1, pp. 100-106, January 1999.
[9] A.K. Stiffler, "Friction and Wear with a Fully Melting Surface," Transactions of ASME, *Journal of Tribology*, vol. 106, pp. 416-419, July 1984.
[10] W.A. Gross, "Film Lubrication," Report RJ117-8, IBM Corp., San Jose, CA, 1960.
[11] *Convective Heat and Mass Transfer*, second edition, W.M. Kays and M.E. Crawford, McGraw-Hill Book Company: New York, 1980.
[12] H.G. Landau, "Heat Conduction in a Meting Solid," *Quart. J. Appl. Math.*, vol. 8, p. 81, 1950.
[13] *Conduction of Heat in Solids*, second edition, H.S. Carslaw and J.C. Jaeger, Oxford at the Clarendon Press, equation 2, p. 63, 1959.
[14] *Conduction of Heat in Solids*, second edition, H.S. Carslaw and J.C. Jaeger, Oxford at the Clarendon Press, equations 34-36, p. 288, 1959.

APPENDIX A. THERMAL BOUNDARY CONDITIONS FOR SOLIDIFICATION ON THE RAIL

The solidification boundary conditions are satisfied by applying the results of a classical solidification problem: the region $x < 0$ initially liquid and the region $x < 0$ solid [14].

The region $x < 0$ has thermal constants $\rho_r, c_r, k_r, \kappa_r$ and is initially at temperature t_{r_o}. The region $x < 0$ is initially liquid with thermal constants ρ, c, k, κ and is initially at temperature t_v. The thermal constants $\rho_s, c_s, k_s, \kappa_s$ of the solidified liquid in the region $0 < x < X$ may be different than the liquid.

The temperatures at time τ of the solid (rail), the solidified layer and the liquid, t_r, t_s and t, respectively, are given by:

$$t_r = AA(1 + erf(\frac{x}{2\sqrt{\kappa_r \tau}})) + t_{r_o}; x < 0 \qquad \text{(A-1)}$$

$$t_s = BB + CCerf(\frac{x}{2\sqrt{\kappa_s \tau}}) + t_{r_o}; 0 < x < X \qquad \text{(A-2)}$$

$$t = t_v - DDerfc(\frac{x}{2\sqrt{\kappa \tau}}); x > X \qquad \text{(A-3)}$$

The position of the interface at time τ is

$$X = 2\lambda\sqrt{\kappa_s \tau} \qquad \text{(A-4)}$$

where

$$\lambda = BZ1\{\frac{\exp(-\lambda)}{BSR + erf(\lambda)} - \frac{BZ\exp(-\lambda ASL)}{BSLerfc(\lambda ASL)}\} \qquad \text{(A-5)}$$

$$\text{AA=BB=BSR}(t_m - t_{r_o})/(BSR + erf(\lambda)) \qquad \text{(A-6)}$$

$$\text{CC} = AA/BSR \qquad \text{(A-7)}$$

$$\text{DD} = (t_v - t_m)/erfc(\lambda \bullet ASL) \qquad \text{(A-8)}$$

$$\text{ASL} = \sqrt{\kappa_s/\kappa} \qquad \text{(A-9)}$$

$$\text{BZ} = (t_v - t_m)/(t_m - t_{r_o}) \qquad \text{(A-10)}$$

$$BZ1=cs(t_m - t_{r_o})/(H_m\sqrt{\pi}) \quad \text{(A-11)}$$

$$BSL=\sqrt{\frac{k_s\rho_s c_s}{k\rho c}} \quad \text{(A-12)}$$

$$BSR=\sqrt{\frac{k_s\rho_s c_s}{k_r\rho_r c_r}} \quad \text{(A-13)}$$

The gradient of t at position x is:

$$\frac{dt}{dx} = DD\,exp(-x^2/4\kappa\tau)/\sqrt{\pi\kappa\tau} \quad \text{(A-14)}$$

The gradient at the interface, $x=X(\tau)$, is:

$$\frac{dt(X(\tau))}{dx} = DDexp(-\lambda^2 \bullet ASL^2)/\sqrt{\pi\kappa\tau} \quad \text{(A-15)}$$

The average value of the gradient at the interface during the contact time is:

$$(\frac{dt(X(\tau))}{dx})_{avg} = 2DDexp(-\lambda^2 \bullet ASL^2)/\sqrt{\pi\kappa\tau} = \frac{2(t_v - t_m)}{\sqrt{\pi\kappa\tau}}(\frac{exp(-\lambda^2\kappa_s/\kappa)}{erfc(\lambda\sqrt{\kappa_s/\kappa})}) \quad \text{(A-16)}$$

The process of solidification of the melt film is considered equivalent to the above solidification process when the average value of the gradient at the melt film matches the above value and the thickness of the solidified layer also matches the thickness assumed for the melt film calculations. The initial liquid temperature, t_v, is used as a parameter to match the gradient at the interface in the two solutions.

APPENDIX B. REVISED LATENT HEAT AND VISCOSITY MODEL

An alloy that exhibits an incipient melting and a liquidus temperature undergoes a phase change in which the energy of transformation is distributed over the range between the two temperatures. The distributed transformation from solid to liquid is also accompanied by a change from the infinite viscosity at incipient melting to the viscosity of the liquid at the liquidus temperature.

Because information on the distribution of the energy is not available, we assumed that it occurs uniformly. The thermal behavior during this melting process can be modeled by adding the latent heat of melting per degree temperature change to the normal specific heat. The extra specific heat applies to both heating and cooling within the range of transformation. We arbitrarily chose the pseudo melting point to be 815 K, 10 K above the incipient melting temperature. The fraction (815-805)/(908-805) = 0.0971 of the latent heat was assumed to occur at this pseudo melting point. The remaining fraction, 0.9029, was distributed uniformly as an increased specific heat between 815 and 908 K. For a latent heat of 3.78×10^5 J/kg, the increase in liquid specific heat is 3670. J/kg/K over this temperature range.

The viscous behavior of the material in this range is more complex. To greatly simplify the problem, it was assumed that the fraction of the energy of transformation corresponds to the local fraction of liquid, then the viscous behavior can be related to a two-phase mixture. The simplest model is that of micro layers of liquid and solid, the thickness of the liquid being ϕ of the total, where ϕ is the liquid fraction. The local viscosity for this configuration is given by $\mu_m = \mu_L/\phi$. In order to retain the basic formulation, we assumed that for $\phi < \phi_0$ the viscosity remains infinite and that the fraction ϕ_0 of the latent heat is concentrated at the corresponding pseudo melting temperature, $t_m' = t_{im} + (t_L - t_{im})\phi_0$ where t_{im} is the incipient melting temperature and t_L is the liquidus temperature. The fraction $1-\phi_0$ of the latent heat is uniformly distributed between t_m' and t_L. Note that for $t_m' = 815$ K, $\phi_0 = 0.0971$. The modified model applies as long as the maximum temperature in the melt film is below t_L.

This model of the phase change process was included in the squeeze film analysis and in the thermal energy equation by finding effective viscosity for a film of thickness h with a parabolic temperature profile using the local viscosity model described above. The effective viscosity for the squeeze film flow is obtained from the solution of the x direction momentum equation neglecting the effect of injection and suction. The value of ϕ can be expressed in terms of y for a parabolic temperature profile, $\theta = 4\theta_C Y(1-Y)$ by

$$\phi = \phi_0 + \left(\frac{b}{4\theta_C}\right)\theta = \phi_0 + \left(1 - \frac{y}{h}\right)\frac{by}{h}$$

where $b = 4\theta C t_m' / (t_L - t_{im})$. Then the momentum equation

$$\frac{\partial p}{\partial z} = \frac{\partial}{\partial y}\left(\mu \frac{\partial u}{\partial y}\right)$$

is integrated for constant $\frac{\partial p}{\partial z}$ using $\mu = \mu L/\phi$ with $u = 0$ at $y = 0$ and $u = 0$ at $y = h$. Comparing the result with the solution to the same equation for $\mu = \mu_L$ gives

$$\mu_S = \mu_L/(\phi_0 + b/10)$$

where μ_S is the effective viscosity for calculating the value of h for squeeze flow using the analysis for uniform viscosity.

A similar process is repeated to find the solution for Couette flow with the same value of ϕ. After one obtains the velocity gradient, one integrates to find the total dissipation. Comparing the result with the same process for $\mu = \mu_L$ gives

$$\mu_Q = \mu/(\phi_0 + b/6)$$

where μ_Q is the effective viscosity used to calculate the viscous heating for Couette flow using a constant viscosity analysis.

Distribution List

Defense Technical Information Center
Administrator
ATTN: DTIC-DDA
8725 John J. Kingman Road, Suite 944
Ft. Belvoir, VA 22060-6218
USA

Mr. David Bauer
IAP Research, Inc.
2763 Culver Ave
Dayton, OH 45429-3723
USA

Mr. Dennis Ladd
U.S. Army TACOM-ARDEC
ATTN: AMSTA-AR-FSP
Picatinny Arsenal, NJ 07806-5000
USA

Mr. Timothy Wolfe
Titan Pulsed Sciences
4855 Ruffner St.- Suite A
San Diego, CA 92111
USA

Dr. Edward Schmidt
U.S. Army Research Laboratory
ATTN: AMSRL-WM-B
Bldg 4600
Aberdeen Proving Ground, MD 21005-5066
USA

Dr. Harry Fair
Institute for Advanced Technology (IAT)
The University of Texas at Austin (UT)
3925 West Braker Lane
Suite 400
Austin, TX 78759-5316
USA

Dr. Keith Jamison
Science Applications Intl. Corp.
PO Box 4216
Fort Walton Beach, FL 32549-4216
USA

Dr. Hans Mark
Institute for Advanced Technology (IAT)
The University of Texas at Austin (UT)
3925 West Braker Lane
Suite 400
Austin, TX 78759-5316
USA

Mr. Alexander Zielinski
U.S. Army Research Laboratory (ARL)
Attn: AMSRL-WM-BC
Bldg 390
Aberdeen Proving Ground, MD 21005-5066
USA

Dr. Ian McNab
Institute for Advanced Technology (IAT)
The University of Texas at Austin (UT)
3925 West Braker Lane
Suite 400
Austin, TX 78759-5316
USA

Dr. John Powell
Ballistic Research Laboratory
ATTN: AMSRL-WT-WD
Bldg 120
Aberdeen Proving Ground, MD 21005-5066
USA

Dr. Jerome Tzeng
US ARMY Research Laboratory
Weapons Technology Directorate
Attn:AMSRL-WM-MB
Aberdeen Proving Ground, MD 21005-5066
USA

Distribution List

Dr. Kuo-Ta Hsieh
Institute for Advanced Technology (IAT)
The University of Texas at Austin (UT)
3925 West Braker Lane
Suite 400
Austin, TX 78759-5316
USA

Dr. Robert Merrill
Institute for Advanced Technology (IAT)
The University of Texas at Austin (UT)
3925 West Braker Lane
Suite 400
Austin, Texas 78759
USA

Dr. Sikhanda Satapathy
Institute for Advanced Technology (IAT)
The University of Texas at Austin (UT)
3925 West Braker Lane
Suite 400
Austin, TX 78759-5316
USA

Mr. Tom Benton
Institute for Advanced Technology (IAT)
The University of Texas at Austin (UT)
3925 West Braker Lane
Suite 400
Austin, TX 78759-5316
USA

Dr. Robert Whalin
U.S. Army Research Laboratory
ATTN: AMSRL-WM-MD
Aberdeen Proving Ground, MD 21005-5066
USA

Dr. William Reinecke
Institute for Advanced Technology (IAT)
The University of Texas at Austin (UT)
3925 West Braker Lane
Suite 400
Austin, TX 78759-5316
USA

Dr. Mark Crawford
Institute for Advanced Technology (IAT)
The University of Texas at Austin (UT)
3925 West Braker Lane
Suite 400
Austin, TX 78759-5316
USA

Dr. William Robinson
Lockheed Martin
Missiles and Fire Control
P.O. Box 650003
Dallas, TX 75265-0003
USA

Mr. Norm Wells
LMMFC
P.O. Box 650003
M/S SP-97
Dallas, TX 75265-0003
USA

Dr. John Mallick
Institute for Advanced Technology (IAT)
The University of Texas at Austin (UT)
3925 West Braker Lane
Suite 400
Austin, Texas 78759
USA